ASIA-PACIFIC JOURNAL OF CHEMICAL ENGINEERING (2016)

Combustion pattern, characteristics and kinetics of biomass and chars from segmented heating carbonization

Kuihua Han[a,b,*], Qian Wang[a], Jianli Zhao[a], K. H. Luo[b,†], Hui Li[a], Yang Chen[b,c], Chunmei Lu[a]

[a]School of Energy and Power Engineering, Shandong University, Jinan 250061, China

[b]Department of Mechanical Engineering, University College London, London WC1E 7JE, UK

[c]Center for Combustion Energy, Tsinghua University, Beijing 100084, China

* Corresponding author. Tel.: +86 531 88392414; fax: +86 531 88392701.

E-mail address: hankh@163.com (K. Han).

† Corresponding author. Tel.: +44 20 7679 3916; fax: +44 20 7388 0180.

E-mail address: k.luo@ucl.ac.uk (K. H. Luo).

Abstract

The combustion patterns, characteristics and kinetics were investigated by thermogravimetric analysis for raw maize straw, cotton stalk, and chars obtained from segmented heating carbonization at 300–800 °C. With increasing carbonization temperature, combustion patterns of biomass chars transform from the sequential reaction steps corresponding to pyrolysis and heterogeneous oxidation of volatiles and char to situ heterogeneous oxidation of fixed carbon and volatiles, the ignition

temperature of biomass chars gradually increase, the ignition index dose not monotonically increase, and the burnout index and combustion characteristic index decrease to different degree. Judging from the combustion characteristic index,chars obtained from 300–500 °C carbonization show better combustibility. The kinetic parameters of raw and carbonized biomass were determined by Coats–Redfern method. Different reaction mechanisms exist in oxidation processes of different chars, which attribute to the synergistic effects of homogenous oxidation of volatiles and heterogeneous oxidation of char. The kinetic parameters obtained from the variation of species and model functions exhibit kinetic compensation effect.

Keywords

Biomass carbonization; combustion pattern; combustion characteristics; combustion kinetics; char

Nomenclature

PID proportional integral derivative

SSR solid state relay

MS maize straw

CS cotton stalk

T_i ignition temperature

D_i the ignition index

TG Thermal Gravity

DTG Differential Thermal Gravity

DTA Differential Thermal Analysis

V_{max} maximum combustion rate

T_{max} corresponding temperature of V_{max}

V_{mean} average combustion rate

T_f burnout temperature

D_f burnout index

S combustion characteristic index

α reaction rate on the extent of reaction

A pre-exponential Arrhenius factor

E activation energy

R gas constant

T temperature

$f(\alpha)$ deferential conversion function,.

β heating rate

$k(T)$ rate constant

n reaction order

$G(\alpha)$ integral conversion function

1. Introduction

Biomass is an alternative carbon-neutral fuel for fossil fuels.Using biomass is considered as an effective countermeasure to reduce carbon dioxide emissions into the atmosphere and mitigate global warming [1, 2]. However, it is a great challenge to replace inexpensive and abundant coal by biomass derived fuels, especially for solid fuel, because of the diversity in the form, calorific value, composition and water content of biomass, and comparative low energy density. These decrease combustion and gasification efficiencies, and enormously enhance the cost of transportation, fuel processing, development and retrofit of power generation equipment and environmental protection facilities.

Consequently, torrefaction and carbonization are more effective energy conversion way to improve biomass fuel quality than densifying and molding, i.e. biomass is pyrolyzed by heating in an inert or oxygen-free environment. The torrefaction temperature is in the range of 200–300 °C [3-5], whereas carbonization is operated at temperatures of 300–500 °C [6]. Torrefied or carbonized biomass char show potential performance on combustion, co-combustion with coal or gasification [7-11], which are based on economical transportation cost, higher energy density, good grindability and combustion characteristics [12]. Torrefaction and carbonization lead to the release of volatile matter from biomass and change the hygroscopic material to hydrophobic one. This transformation improves the reactivity of solid biomass. Bridgeman et al. [13] studied the difference of burning profiles of raw and torrefied reed canary grass by thermogravimetric analysis. It indicated that the higher of torrefaction temperatures, the

higher heats of reactions and the higher temperatures of start point for mass loss during the torrefied products combustion. In addition, the behavior of the raw and torrefied willow were also studied in a methane–air flame under conditions of high heating rate and temperature, and it was found that the higher of torrefaction temperatures, the shorter of volatile combustion time, the longer of char burnout times for torrefied biomass, and the shorter of average ignition times for volatile and char combustion. Pimchuai et al. [14] investigated rice husk reaction in a spout-fluid bed combustor, and reported that torrefied rice husk ignited faster and raised the bed temperature to a higher level when compared to raw rice husk. These changes of ignition were very likely due to the low moisture content in the torrefied willow and rice husk.Du et al. [9] evaluated the utility potential of pretreated biomass in blast furnaces, the pretreatment temperatures of which were between 250 and 500 °C.It indicated that the energy densities of bamboo and madagascar almond were improved drastically from carbonization, whereas the increase in the calorific value of pretreatment rice husk from the pretreatment was not obvious. Carbonization at higher temperatures significantly increases ignition temperature of the char, but decreases burnout. The fuel properties of pretreated biomass materials are superior to those of the low-volatile coal, which can be blended with coals for pulverized coal injection.

In consideration of high moisture content of raw biomass and lower heating cost of the process, a new three-step carbonization equipment was developed. The initial heating of this carbonization equipment only needs a little external supply of oil or gas

due to the characteristics of self-heating by burning the gas produced from the pyrolyzing process. The heating process of segmented design contributes to higher mass and energy yields than constant heating rate and/or constant temperature heating [15].

Although the combustion characteristics of torrefied or low temperature carbonized biomass were investigated, few studies focused combustion characteristics of higher temperature carbonized biomass and evolution from raw biomass to the chars. The purposes of the present study are to explore the combustion patterns, characteristics and kinetics of charsobtained fromsegmented heating carbonization at final temperature 300–800 °C.The results from this paper will contribute to theoretical basis of biomass chars combustion and the burning performance in furnace of which are beyond the scope of this paper.

2. Experimental

2.1. Carbonization process

A schematic of the three-step carbonization equipment system and procedure is shown in Fig. 1a [15]. The material can be conveyed by screw conveyers at adjustable feed rates, meanwhile it can be heated by three segmented furnace in the order of low to high temperature. The length and inner diameter of each furnace are 400 cm and 50 cm respectively. The flame temperature of the smokeless combustion device can be controlled up to 1200 °C by self-pyrolysis gas and external supply of oil or gas, accordingly heating temperature from over 800 °C in the bottom furnace for producing carbonaceous material with different performance [15].

To simulate the segmented heating process, the carbonization experiment system, as shown in Fig.1b, was made up of a nitrogen steel cylinder, a rotameter, a reactor and a product gas treatment unit. The steel cylinder was used to supply nitrogen for providing inert atmospheres. The volumetric flow rate of nitrogen was controlled by the rotameter. The reactor comprised a corundum tube with sealing flanges and an electrical heating element with temperature controller. The inner diameter and the length of the tube were 10 cm and 80 cm respectively, and the length of constant temperature zone is 20 cm, which is enough for an alundum crucible get heated as evenly as possible at the specified temperature. The both ends of flanges were welded with stainless pipes to transport the nitrogen and product gas, the inner diameter of which was 10 mm. The electrical element of the furnace was composed of silicon carbide rods with rated power of 3 kW. The reaction temperature, from room temperature to 1500 °C, was controlled by a proportional integral derivative (PID) temperature controller, and the power of the heater was controlled by a solid state relay (SSR) power controller. The samples were placed in the combustion boat for carbonization and the heater was used to elevate and sustain the reaction temperature. In the product gas treatment unit, a conical flask was employed to remove tar and clean exhaust gas. Heating temperature profiles at various final temperatures of this segmented heating carbonization simulator are shown in Fig. 2.

Fig.1

Fig.2

148 2.2. Experimental procedure

149 Before experiments were carried out, the received biomass was dried in an oven at
150 temperature of 105 °C for 20 hours, then the air dried biomass was ground into powders
151 by a blade pulverizer. The powders were sieved by a vibrating screen. The particle sizes
152 of the tested samples were controlled between 85 and 200 mesh (i.e. 74–180 μm). The
153 sieved biomass was dried again at 105 °C for 10 h to provide basic samples material for
154 analysis and experiments.

155 In each batch, the pulverized powder with the total mass of 10 g (±10%) was placed
156 in an alundum crucible, which was calcined, cooled and stored in a desiccator, and
157 weighed in advance. After the crucible with sample was placed in the tube, then the
158 flanges were tightened, the valve was opened with the flow rate of nitrogen at 2 L/min
159 (25 °C). It was continuously blown into the reaction tube for 20 minutes to keep the
160 sample in an inert environment, the electrical furnace was input power, and then the
161 sample was heated by programmed temperature controlling instrument, as shown in Fig.
162 2. The heating time was 5 min and the duration time was 15 min every segment. The
163 exhaust left from the reactor, were cooled and washed in the conical flask during the
164 total heating and cooling process. The nitrogen was not stopped until the furnace
165 temperature decrease to 150 °C, and the crucible and sample were moved towards right
166 sideof the tube at lower temperature zone by opening the right flange. Finally, the
167 crucible and sample were removed to a desiccator, cooled to room temperature and
168 weighed. The experiment under any given condition was usually carried out more than

169 twice. The results were fairly uniform between each batch and the relative error was less
170 than 5%. The carbonized products were saved in sample bottles for analysis and further
171 experiments.

172 **2.3. Samples**

173 Two agricultural crops, namely maize straw (MS), cotton stalk (CS), respectively,
174 have been air dried and carbonized with subsequent analysis of the solid residues. These
175 herbaceous and lignocellulose biomass material are representatively used for biomass
176 briquette fuel, heat and power generation, and heating and cooking in rural areas of
177 North China, which were grown at rural areas in Dezhou, Shandong province.

178 In this study, the raw and carbonized biomass were all analyzed. The measurements
179 include proximate, elemental (ultimate) analysis, calorific value. The proximate analysis
180 was performed in accordance with the standard procedure of American Society for
181 Testing and Materials. The volatile analyses were conducted in an auto volatile analyzer
182 (CKIC 5E-MAG6600). The elemental analysis was carried out using an elemental
183 analyzer (LecoTruSpec CHN) and sulfur analyzer (Leco S144DR). The higher heating
184 values (HHVs) of the samples were measured by a bomb calorimeter (CKIC
185 5E-AC8018). The fuel property analysis of two raw samples and chars are listed in
186 Table 1.

187 **Table 1**

188 **2.4. Thermogravimetric analysis**

189 2.4.1. Equipment and process

Burning profiles of samples were performed using a microcomputer differential thermal balance analyzer (HCT-3 Series made by Beijing Henven Scientific Instrument Factory). A sample mass of 5 mg is used in this study. The combustion of all the samples was carried out at a heating rate of 10 °C/min under air flowing rate of 50 ml/min and protective gas flow of nitrogen is 50 ml/min. The final temperature was 800 °C, with a holding time of about 80 min. The heating rate of this order is generally considered able to ensure that no temperature gap exists between the sample and its surroundings [16]. Both thermogravimetric and differential temperature measurements were recorded simultaneously during combustion analysis as a function of heating time. From the sample mass-loss percentage, the normalized mass-loss ratio of a sample can be determined and plotted versus the sample temperature as the TG curve. The DTG curve can then be calculated by differentiating the mass-loss ratio with respect to time or temperature.

2.4.2. Experimental data process

In order to analyze the combustion characteristics of raw and carbonized biomass, a series of parameters were defined and calculated by thermogravimetric analysis, including the ignition temperature (T_i), the ignition index (D_i), the maximum combustion rate (V_{max}), the corresponding temperature of V_{max} (T_{max}), the average combustion rate (V_{mean}), the burnout temperature (T_f), the burnout index (D_f) and the combustion characteristic index (S). The lower the ignition temperature, the better the combustion reactivity. The bigger the combustion rate, the ignition index, the burnout

index, and the value *S*, the higher the combustion activity of fuel.

The ignition temperature, the maximum combustion rate (i.e. the maximum of the mass loss rate during the combustion process), and the corresponding temperature of V_{max}, were defined in the literature [17]. The burnout temperature (T_f) was defined as the temperature at which the mass loss rate is smaller than –0.01mg/min.

Due to the effects of different heating methods on the ignition of fuels were slight; the ignition time cannot completely reflect ignition characteristic of the samples. The ignition index (D_i) is determined by the equation as follows [18] to evaluate the ignition characteristic:

$$D_i = \frac{V_{max}}{t_p t_i} \qquad (1)$$

where t_p and t_i are the correspondingtime of the maximum combustion rate and ignition temperature, respectively.

The average combustion rate (V_{mean}) represents the average weight loss rate during the entire combustion process, it is determined by the equation as follows:

$$V_{mean} = \frac{W_1 - W_2}{t} \qquad (2)$$

Where W_1 is the sample mass at T_i, $W_2$is the sample mass at T_f, and t is the time zone from T_i to T_f.

Also the burnout index is used to evaluate the burnout performance, which can be described as follows[19]to evaluate the burnout characteristic:

$$D_f = \frac{V_{max}}{\Delta t_{1/2} t_p t_f} \qquad (3)$$

Where $\Delta t_{1/2}$ the time zone of $(dw/dt)/V_{max}=1/2$, t_f is the burnout time.

The combustion characteristic index (S) is determined by the equation as follows [20,21]:

$$S = \frac{V_{\max} \times V_{\text{mean}}}{T_{\text{i}}^2 \times T_{\text{f}}} \quad (4)$$

3. Results and discussion

3.1. Combustion pattern

There are two extreme solid fuel conversion pathways in an oxidizing atmosphere. One is represented bythe sequential reaction steps corresponding to pyrolysis of the material and heterogeneous oxidation of volatiles and char generated by pyrolysis (Case I). The other represents direct in situ heterogeneous oxidation of fixed carbon and volatile matter that ultimately yield combustion products (Case II). How close the actual conversion pathway to either extreme is depended on the very nature of the solid fuel and on operating conditions (particle size, temperature, and oxygen partial pressure) [22]. In fact, there is a pattern typical of a reaction pathway (Case III) intermediate between the two extreme Case I and Case II. Senneca et al. [22] analyzed the three cases by the comparison of the derivative curves obtained from thermogravimetric analysis of either inert or oxy-pyrolysis. Alternatively, reaction pathways can be judged by comparison of peaks of the Differential Thermal Gravity (DTG) and Differential Thermal Analysis (DTA) curves at low heating rate (such as 10–15 °C/min) because there is significant exothermic difference between pyrolysis [23, 24] and situ heterogeneous oxidation of the material. Consequently, the three cases also can be described by DTG curve and DTA curve obtained from thermogravimetric analysis of

253 combustion. Three different situations are possible:

254 (Case I) The DTG curve exhibits two peaks. The first, a larger one, represents the
255 release of volatiles by pyrolysis at lower temperature, which corresponds to a smaller
256 first heat release peak of DTA curve. The second, a smaller one, represents char
257 combustion at higher temperature, which corresponds to a certain heat release peak of
258 DTA curve. The influence of oxidizing atmosphere on the course of pyrolysis is likely to
259 be absent or negligible. Pure thermal degradation of the fuel is indeed faster than its
260 heterogeneous oxidation.

261 (Case II) The DTG curve exhibits only one large peak, which represents direct in
262 situ heterogeneous oxidation of fixed carbon and volatiles at higher temperature, and
263 corresponds to a large heat release peak of DTA curve. The raw fuel burns faster than its
264 pyrolysis in the case.

265 (Case III) The DTG curve exhibits two peaks. The first peak is possibly with a
266 combustion of volatiles, which corresponds to a larger or broad heat release peak of
267 DTA curve. The second peak at higher temperature is related to char combustion. This is
268 a pattern typical of a reaction pathway intermediate between the two extreme cases I
269 and Case II. The pattern of case III is instead indicative of synergistic effects of purely
270 thermal degradation and heterogeneous oxidation, occurring over comparable time
271 scales. In this case the release of volatile matter is enhanced by the mild heterogeneous
272 oxidation and oxygen-promoted bond cleavage. The very chemical nature of pyrolytic
273 processes will be affected accordingly. This process should not be confused with

thermal feedback to the particle of heat released by homogeneous combustion of volatile matter. This is possible only once pyrolysis is fully active and volatile matter has ignited [22].

Fig.3 and 4 shows TG, DTG and DTA profiles of combustion of the raw/carbonized maize straw and cotton stalk, respectively. From these curves, the evolution from case I, Case III to Case II orderly are presented by the different raw biomass and chars obtained from 300–800 °C carbonization. The combustion patterns of raw biomass and 300-char approximately accord with the Case I, the volatiles content of which is higher than 56.72%, as listed in Table 1. A pattern typical of the Case II occurs in the oxidation of 800-char with much lower volatiles percentage. The conversion pathways of 400-char and 500-char belong to the Case III inclined to the Case I, the volatiles content of which is in the range of 21.79%–37.06%. The first peaks of DTG and DTA curves of 400-char and 500-char are broader or lower corresponding to mainly the release and homogeneous combustion of volatile matter in the Fig. 3 and 4. By comparison, the conversion pathways of 600-char and 700-char belong to the Case III inclined to the Case II. The first peaks of DTG and DTA curves of 600-char and 700-char are larger, which are affected synergistically by the homogeneous combustion of volatile matter and the heterogeneous oxidation of char. Accordingly, the second peaks of DTG and DTA curves of 600-char and 700-char are smaller than those of 400-char and 500-char. With the increase of carbonization temperature, this shift is more noticeable for chars obtained from 400–700 °C carbonization. It should be noted that the evolution of the

conversion pathways is explained not only by the reduction of volatiles, but also by the change of particle size, BET surface area and porosity, which are caused by carbonization at different temperatures.

Fig. 3

Fig. 4

3.2. Combustion characteristic parameters

On the basis of thermogravimetric analysis, the combustion characteristic parameters are calculated and listed in Table 2. The quantitative characteristic temperatures and indexes can contribute to judge the performances of solid fuel combustion. The ignition temperatures of the obtained chars gradually increase with the carbonization temperature, which generally accords with the reduction of volatiles of the obtained chars. However, the ignition index does not monotonically increase with increasing temperature. It can be explained by two reasons. One reason is that the start point for mass loss during combustion occurs at increasingly higher temperatures for the obtained chars at higher carbonization temperatures. The other reason is that changes of the maximum combustion rates corresponding to the volatiles or char result from the shift of conversion pathways as analyzed above. The burnout temperature are increased with the increase of fixed carbon content, as shown in Table 2, while the burnout index decreases significantly. The extent of variation is little for the average combustion rate. Although the combustion characteristic index decrease with increasing carbonization temperatures, the values *S* of chars obtained from 300–500 °C carbonization is close to

316 that of raw biomass. In all, the obtained chars show satisfying combustibility.

317 **Table 2**

318 **3.3. Kinetic parameters**

319 The temperature dependence of heterogeneous solid-state reactions may be described

320 by the Arrhenius equation [25, 26]:

321 $$\frac{d\alpha}{dt} = A\exp(-\frac{E}{RT})f(\alpha) \quad (5)$$

322 where t is time, α is the reaction rate on the extent of reaction, A is the pre-exponential

323 Arrhenius factor, E the activation energy, R the gas constant and T the temperature. $f(\alpha)$

324 is the deferential conversion function, which characterizes the reaction mechanism.

325 In non-isothermal kinetics, for the most usual case of a linear heating program the

326 heating rate is constant (β=dT/dt=constant), the above expression can be transformed

327 into differential equation:

328 $$\frac{d\alpha}{dT} = \frac{1}{\beta}k(T)f(\alpha) = \frac{A}{\beta}\exp\left(-\frac{E}{RT}\right)f(\alpha) \quad (6)$$

329 where $k(T)$ is the rate constant. Among the mathematical assumptions to explain the

330 solid reaction mechanism, the Coats–Redfern method, which assumes $f(\alpha) =$

331 $(1-\alpha)^n$ to be the reaction model and n is the reaction order, has been broadly used.

332 Through variable separation and integration, Eq. (6) leads to

333 $$G(\alpha) = \int_0^\alpha \frac{d\alpha}{(1-\alpha)^n} = \frac{A}{\beta}\int_0^T \exp\left(-\frac{E}{RT}\right)dT \quad (7)$$

334 where $G(\alpha)$ is the integral conversion function. The integral on the right-hand side of Eq.

335 (7) leads to

336 $$\int_0^\alpha \frac{d\alpha}{(1-\alpha)^n} = \frac{ART^2}{\beta E}\left(1-\frac{2RT}{E}\right)\exp\left(-\frac{E}{RT}\right) \quad (8)$$

Taking logarithms for both side of Eq. (8) leads to

$$\ln\left[\frac{-\ln(1-\alpha)}{T^2}\right] = \ln\left[\frac{AR}{\beta E}(1-\frac{2RT}{E})\right] - \frac{E}{RT} \qquad (n=1) \qquad (9)$$

$$\ln\left[\frac{1-(1-\alpha)^{1-n}}{T^2(1-n)}\right] = \ln\left[\frac{AR}{\beta E}(1-\frac{2RT}{E})\right] - \frac{E}{RT} \qquad (n\neq 1) \qquad (10)$$

Since in general $\frac{E}{RT} \gg 1$ and it exhibits a small variation with *T*, for practical considerations it is assumed that the term $(1-\frac{2RT}{E})$ is approximately constant, i.e.$1-\frac{2RT}{E} \approx 1$, thus the Eq. (9) and (10) can be reduced by

$$\ln\left[\frac{-\ln(1-\alpha)}{T^2}\right] = \ln\frac{AR}{\beta E} - \frac{E}{RT} \qquad (n=1) \qquad (11)$$

$$\ln\left[\frac{1-(1-\alpha)^{1-n}}{T^2(1-n)}\right] = \ln\frac{AR}{\beta E} - \frac{E}{RT} \qquad (n\neq 1) \qquad (12)$$

The plot of $\ln\left[\frac{-\ln(1-\alpha)}{T^2}\right]$ $(n=1)$or $\ln\left[\frac{1-(1-\alpha)^{1-n}}{T^2(1-n)}\right]$ $(n\neq 1)$*vs.* $\frac{1}{T}$ gives a straight line whose slope $(-\frac{E}{R})$ and intercept $(\ln\frac{AR}{\beta E})$ allow an estimation of the values of the activation energy (*E*) and pre-exponential factor (*A*), respectively. In the previous research [27, 28], *n*=1 was generally assumed for raw biomass or blended with coal combustion. However, as analyzed above, combustion patternsare more diversified for the very nature of the solid fuel. The regression line corresponding to different ranges of temperature could be achieved and the reaction order of *n* is optimized from 0.33, 0.5, 0.67, 1, 1.25, 1.5 and 2 in this study. The correlation coefficient (*R*) is the selection criterion for the proper reaction order, which is ascertained as the good satisfaction of the linear regression. Then, the kinetic parameters can be calculated. The deduced data are given in Table 3 and the kinetic parameters are calculated for different temperature zones which are approximately divided by the main weight loss regions on each DTG curve.

Table 3

From Table 3, it is observed that there are different reaction mechanisms for the oxidation processes of different samples, and even for different reaction stages ofacertain oxidation process. Corresponding to the oxidation pathways of Case I, the reactions of first regions are based on the first-order reaction for the most of samples, which is in accordance with the literature [29-31]. Gao et al. [29, 30] obtained the activation energy of 52.9–184.2 kJ/mol of raw and treated wood under the same experimental conditions. Yorulmaz and Atimtay [31] obtained the activation energy of 44.58–53.67 kJ/mol of three kinds of raw biomass under the same heating rate and reaction mechanisms. For oxidation situation of Case II, the mechanism of chars obtained from 800 °C carbonization accords with those of bio-char and coal-char. Blasi et al. [32] obtained the activation energy of 83.2–100.4 kJ/mol for four kinds of biomass chars by a single kinetic model of combustion under the non-isothermal conditions (heating rates of 10 K/min and a final temperature of 873 K). Kök [33] studied the combustion of different rank coal by differential scanning calorimetry and thermogravimetry. It was observed that the activation energies of samples were varied inthe range of 66.5–92.0 kJ/mol in Arrhenius and 54.0–88.0 kJ/mol in Coats and Redfern methods respectively. The obtained activation energy in present study is inconsistency in two different methods. The mechanism of the chars obtained from 400–700 °C carbonization, corresponding to Case III, show diversity at different reaction regions. The reactions of first regions are two-order reaction for MS-chars

obtained from 400–600 °C carbonization. It can be explained by synergistic effects of pure thermal degradation and oxidation, occurring over comparable time scales. The exponent n of the second and third regions corresponding to Case III varies with the nature of the obtained chars, possibly even involving the secondary decomposition and oxidation of tar deposited in chars. Because of the different nature of biomass and coal chars, diverse reaction orders were obtained by modeling the combustion of homogenous and heterogeneous chars as a single reaction in the previous study [32, 34]. Besides the influence of the nature of chars, the kinetics of different reaction regions are synthetically effected by the reaction temperature, the development of surface area as combustion proceeds, and the increase in the ratio of ashes (catalytically active) to the obtained char.

3.4. Kinetic compensation effect

Although the activation energy does not increase monotonously with the increase of carbonization temperatures for different exponent *n* and mechanism, as Table 3 shows, it should be noted that anincrease in the activation energy accompanies with an increase in the pre-exponential factor. A linear dependence between the values of ln*A* and *E* (ln$A$=0.1743E–0.5079; R^2=0.9959) has been observed for all kinetic parameters in Table 3. The high linearity between ln*A* and *E* indicates the existence of kinetic compensation effect. It is noted that the kinetic compensation effect results from the species variation and mechanism model variation. According to this relationship, for any changes in experimental activation energy arising from the experimental conditions, a

corresponding change *A* also occurs, thus we could correlate the different parameters under different experimental conditions [35]. Therefore, it is possible that the introduction of compensation effect may act as a tool for check-up in the kinetic calculation for materials of similar reactivity [36, 37], and provide a possible means to predict the effects of experimental factors on kinetic parameters. If available, it will be useful for the modeling of biomass char combustion. In this study, the kinetic parameters of different biomass and chars have been significantly incorporated into the compensation effect. It indicates that the calculated kinetic parameters corresponding to model functions and reaction regions are rational to a certain extent. The comparison and check-up of the kinetic parameters with other study is also worth further investigating.

4. Conclusions

The combustion patterns, characteristics and kinetics were investigated by thermogravimetric analysis for raw maize straw, cotton stalk, and chars obtained from segmented heating carbonization at 300–800 °C. With increasing carbonization temperature, the combustion patterns from biomass to chars transform from the sequential reaction steps corresponding to pyrolysis and heterogeneous oxidation of volatiles and char to situ heterogeneous oxidation of fixed carbon and volatiles, the ignition temperature of biomass chars gradually increase, the ignition index dose not monotonically increase, and the burnout index and combustion characteristic index decrease to different degree. Judging from the combustion characteristic index, chars

obtained from 300–500 °C carbonization show better combustibility. Different reaction mechanisms exist in oxidation processes of different chars. The kinetic parameters obtained from the variation of species and model functions exhibit kinetic compensation effects.

Acknowledgements

This study was supported by the National Natural Science Foundation of China (51206096) and College Independent Innovation Fund of Jinan (201401275).

References

1. Demirbas A. Combustion characteristics of different biomass fuels, Prog. Energy Combust. Sci. 30(2004) 219–230.

2. Libra JA, Ro KS, Kammann C, Funke A, Berge ND, Neubauer Y, Titirici MM, Fühner C,Bens O,Kern J,Emmerich KH. Hydrothermal carbonization of biomass residuals: a comparative review of the chemistry, processes and applications of wet and dry pyrolysis, Biofuels 2 (2011) 71–106.

3. Peng JH, BiXT, Lim CJ,Sokhansanj S. Study on density, hardness, and moisture uptake of torrefied wood pellets, Energy Fuel 27(2013) 967–974.

4. Sabil KM, Aziz MA, Lal B,UemuraY. Synthetic indicator on the severity of torrefaction of oil palm biomass residues through mass loss measurement, Appl. Energy 114 (2014) 104–113.

5. Chen WH, Peng JH, Bi XT.A state-of-the-art review of biomass torrefaction, densification and applications. Renew. Sust. Energ. Rev. 44(2015)847-866.

442 6. Abdullah H, Wu HW. Biochar as a fuel: properties and grindability of biochars
443 produced from the pyrolysis of mallee wood under slow-heating conditions, Energy
444 Fuel 23 (2009) 4174–4181.
445 7. Deng J,Wang G,Kuang J, Zhang Y, LuoY. Pretreatment of agricultural residues for
446 co-gasification via torrefaction, J. Anal. Appl. Pyrol. 86(2009) 331–337.
447 8. Chen WH,Cheng WY, Lu KM, Huang YP. An evaluation on improvement of
448 pulverized biomass property for solid fuel through torrefaction, Appl. Energy 88(2011)
449 3636–3644.
450 9. Du SW, Chen WH, Lucas JA. Pretreatment of biomass by torrefaction and
451 carbonization for coal blend used in pulverized coal injection, Bioresour. Technol.
452 161(2014) 333–339.
453 10. Lu KM, Lee WJ, Chen WH, Liu SH, Lin TC. Torrefaction and low temperature
454 carbonization of oil palm fiber and eucalyptus in nitrogen and air atmospheres,
455 Bioresour. Technol. 123(2012)98-105.
456 11. Wijayanta AT, Alam MS, Nakaso K, Fukai J, Kunitomo K, Shimizu M.,
457 Combustibility of biochar injected into the raceway of a blast furnace, Fuel Process.
458 Technol. 117 (2014) 53–59.
459 12. Van der Stelt MJC, Gerhauser H, Kie lJHA, Ptasinski KJ. Biomass upgrading by
460 torrefaction for the production of biofuels: A review, Biomass Bioenergy 35 (2011)
461 3748–3762.
462 13. Bridgeman TG, Jones JM, Shield I, Williams PT. Torrefaction of reed canary grass,

463 wheat straw and willow to enhance solid fuel qualities and combustion properties. Fuel
464 87(2008) 844–856.
465 14. Pimchuai A, Dutta A, Basu P. Torrefaction of agriculture residue to enhance
466 combustible properties, Energy Fuels 24(2010) 4638–4645.
467 15. Du J, Sun L, Zhang Y, Ueno M, Kawamithi H.A study of technological parameters
468 for agricultural three-step carbonization equipment, Mach. Des. Manu. 12 (2010)
469 186–188.
470 16. Bilbao R, Mastral JF, Aldea ME, Ceamanos J, Kinetic study for the thermal
471 decomposition of cellulose and pine sawdust in an air atmosphere, J. Anal. Appl. Pyrol.
472 39 (1997) 53–64.
473 17. Niu S, Han K, Lu C. Release of sulfur dioxide and nitric oxide and characteristic of
474 coal combustion under the effect of calcium based organic compounds, Chem. Eng. J.
475 168 (2011) 255–261.
476 18. Li X, Ma B, Xu L, Hu Z, Wang X. Thermogravimetric analysis of the
477 co-combustion of the blends with high ash coal and waste tyres, Thermochimica Acta
478 441(2006) 79–83.
479 19. Gong X, Guo Z, Wang Z, Reactivity of pulverized coals during combustion
480 catalyzed by CeO_2 and Fe_2O_3, Combust. Flame 157(2010) 351–356.
481 20. Nie QH, Sun SZ, Li ZQ. Thermogravimetric analysis on the combustion
482 characteristics of brown coal blends, Combust. Sci. Technol. 7 (2001)71–76.
483 21. Luo SY, Xiao B, Hu ZQ, Liu SM, Guan YW. Experimental study on

484 oxygen-enriched combustion of biomass micro fuel, Energy 34(2009) 1880–1884.
485 22. Senneca O, Chirone R, Salatino P.A thermogravimetric study of nonfossil solid
486 fuels. 2. Oxidative pyrolysis and char combustion. Energy Fuels 16 (2002) 661–668.
487 23. Yang H, Yan R, Chen H, Lee DH, Zheng C, Characteristics of hemicellulose,
488 cellulose and lignin pyrolysis, Fuel 86 (2007) 1781–1788.
489 24. Chen Q, Yang R, Zhao B, Li Y, Wang S, Wu H, Zhuo Y, Chen C. Investigation of
490 heat of biomass pyrolysis and secondary reactions by simultaneous thermogravimetry
491 and differential scanning calorimetry, Fuel 134 (2014) 467–476.
492 25. Lopez-Fonseca R, Landa I, Gutierrez-Ortiz MA, Gonzalez-Velasco JR.
493 Non-isothermal analysis of the kinetics of the combustion of carbonaceous materials, J.
494 Therm. Anal. Calorim. 80 (2005) 65–69.
495 26. Otero M, Calvo LF, Gil MV, García AI, Morán A. Co-combustion of different
496 sewage sludge and coal: A non-isothermal thermogravimetric kinetic analysis, Bioresour.
497 Technol. 99 (2008) 6311–6319.
498 27. Liang XH, Kozinski JA. Numerical modeling of combustion and pyrolysis of
499 cellulosic biomass in thermogravimetric systems, Fuel 79 (2000) 1477–1486.
500 28. Wang C, Wang F, Yang Q, Liang R. Thermogravimetric studies of the behavior of
501 wheat straw with added coal during combustion, Biomass Bioenergy 33 (2009) 50–56.
502 29. Gao M, Pan DX, Sun CY. Resin and Amino Resin modified with phosphoric acid
503 study on the thermal degradation of wood treated with amino, J. Fire Sci. 21 (2003)
504 189–201.

505 30. Gao M, Li SY, Sun CY. Thermal degradation of wood in air and nitrogen treated
506 with basic nitrogen compounds and phosphoric acid, Combust. Sci. Tech. 176 (2004)
507 2057–2070.
508 31. Yorulmaz SY, Atimtay AT. Investigation of combustion kinetics of treated and
509 untreated waste wood samples with thermogravimetric analysis. Fuel Process. Technol.
510 90 (2009) 939–946.
511 32. Blasi CD, Buonanno F, Branca C.Reactivities of some biomass chars in air, Carbon
512 37 (1999) 1227–1238.
513 33. Kök MV. Temperature-controlled combustion and kinetics of different rank coal
514 samples, J. Therm. Anal. Calorim. 79(2005) 175–180.
515 34. Kastanaki E, Vamvuka D. A comparative reactivity and kinetic study on the
516 combustion of coal–biomass char blends, Fuel 85(2006) 1186–1193.
517 35. Prasad TP, Kanungo SB, Ray HS, Non-isothermal kinetics: some merits and
518 limitations, Thermochimica Acta 203(1992) 503–514.
519 36. Mui ELK, Cheung WH, Lee VKC, McKay G. Compensation effect during the
520 pyrolysis of tyres and bamboo, Waste Manage 30 (2010) 821–830.
521 37. Dong Q, Xiong Y. Kinetics study on conventional and microwave pyrolysis of
522 moso bamboom, Bioresour. Technol. 171 (2014) 127–131.
523

Table 1

Proximate analysis, ultimate analysis and heating values of biomass and char (by wt. dry basis)

samples	Proximate analysis (%)			Ultimate analyses (%)					Heating values (MJ/kg)	Mass yields (%)
	A	V	FC	C	H	O	N	S	HHV	Y_M
MS	7.67	75.66	16.67	47.03	7.01	36.34	1.68	0.28	19.02	–
MS-300-Char	11.00	63.15	25.84	52.32	5.75	29.13	1.52	0.28	21.50	64.50
MS-400-Char	18.29	37.06	44.65	58.29	4.50	16.84	1.79	0.29	22.12	38.28
MS-500-Char	25.52	22.81	51.67	56.02	3.58	13.06	1.54	0.27	23.04	31.16
MS-600-Char	26.13	18.80	55.08	58.40	2.99	10.51	1.74	0.24	23.85	29.92
MS-700-Char	24.24	12.15	63.61	66.51	2.71	4.62	1.68	0.24	25.12	29.64
MS-800-Char	24.04	8.94	67.02	67.93	2.23	3.80	1.75	0.25	25.37	29.03
CS	10.69	70.82	18.49	47.35	6.42	33.95	1.26	0.33	18.02	–
CS-300-Char	15.15	56.72	28.13	52.03	5.16	25.83	1.48	0.36	21.87	66.37

CS-400-Char	23.61	28.00	48.39	62.66	4.01	7.79	1.54	0.40	23.96	40.63
CS-500-Char	26.97	21.79	51.24	60.18	3.08	8.21	1.16	0.40	23.86	34.94
CS-600-Char	30.49	17.62	51.89	58.17	2.45	7.09	1.40	0.40	23.41	34.87
CS-700-Char	27.17	8.94	63.89	67.45	2.10	1.43	1.45	0.40	25.18	34.55
CS-800-Char	28.27	9.51	62.22	66.84	1.75	1.04	1.75	0.35	24.14	33.13

Table 2

Combustion characteristics parameters of raw biomass and chars

Samples	T_i (°C)	t_i (min)	D_i (10^{-3})	T_{max} (°C)	t_p (min)	V_{max} (mg/min)	Δt (min)	T_f (°C)	t_f (min)	D_f (10^{-4})	V_{mean} (mg/min)	S (10^{-9})
MS	263.2	18.0	1.32	449.1	35.9	0.850	0.6	460.2	37.1	10.64	0.176	4.69
MS-300-char	276.7	25.9	0.78	450.6	42.8	0.861	0.8	474.2	45.4	5.54	0.187	4.43
MS-400-char	319.5	27.1	1.07	448.5	39.9	1.161	1.1	481.7	43.3	6.11	0.178	4.20
MS-500-char	331.2	27.1	1.24	448.7	38.2	1.280	1.4	489.8	42.9	5.58	0.175	4.17
MS-600-char	341.3	31.4	1.18	349.2	31.9	1.180	2.2	497.6	47	3.58	0.168	3.42
MS-700-char	350.3	25.4	1.67	366.2	26.3	1.113	5.8	501.8	40.4	1.81	0.172	3.10
MS-800-char	352.9	26.1	1.50	368.2	27.1	1.061	6.3	505.5	41.5	1.50	0.166	2.80
CS	265.7	23.1	0.99	429.3	38.6	0.883	0.6	452	41.2	9.25	0.171	4.73
CS-300-char	271.2	22.9	1.17	425.6	37.7	1.009	0.9	472.8	42.9	6.93	0.161	4.67

CS -400-char	296.2	25.8	1.27	426.1	38.0	1.245	1.3	491.2	44.9	5.61	0.152	4.40
CS -500-char	301.5	23.2	1.56	423.7	34.6	1.252	1.4	494.6	42.1	6.14	0.152	4.22
CS -600-char	335.9	27.4	1.61	361.1	29.6	1.307	2.1	506.5	44.3	4.75	0.165	3.76
CS -700-char	336.8	29.7	1.20	370.9	32.3	1.151	1.9	514.4	47.3	3.97	0.152	3.01
CS -800-char	347.1	29.2	1.22	360.8	30.3	1.078	6.8	521.8	46.6	1.12	0.159	2.73

Table 3

Combustion kinetic parameters of samples

Samples	Temperature range(℃)	Reaction Order *n*	Fitting formula	Activation energy *E*(kJ/mol)	Pre-exponential factor *A*(s^{-1})	Correlation coefficient *R*	Standard deviation
MS	200-323	1	y=4.7047-10364.7503x	86.2	1.14E+07	0.9980	0.0831
	323-443	1	y=-9.9115-1672.279x	13.9	8.29E-01	0.9982	0.0082
	443-477	1.5	y=70.2884-58578.2392x	487.0	1.97E+36	0.9871	0.1622
MS-300-Char	223-316	1	y=12.3470-15125.8451x	125.8	3.48E+10	0.9965	0.1170
	316-443	1	y=-8.7918-2592.0146x	21.6	3.94E+00	0.9942	0.0245
	443-480	1.5	y=43.1026-39448.3277x	328.0	2.07E+24	0.9895	0.1086
MS-400-Char	267-443	2	y=3.4300-10790.8426x	89.7	3.33E+06	0.9825	0.2659
	443-493	1.5	y=55.5499-48899.1807x	406.5	6.52E+29	0.9932	0.1404

MS-500-Char	267-433	2	y=4.1469-11569.6259x	96.2	7.32E+06	0.9981	0.0891
	433-483	1.25	y=25.6615-27307.852x	227.0	3.81E+16	0.9975	0.0483
MS-600-Char	338-369	2	y=33.7006-29822.8600x	248.0	1.29E+20	0.9996	0.0234
	369-444	1.25	y=-6.0240-4520.6965x	37.6	1.09E+02	0.9994	0.0077
	444-491	1.5	y=43.3925-39942.1723x	332.1	2.80E+24	0.9935	0.1104
MS-700-Char	286-347	1	y=-0.4103-9261.7043x	77.0	6.14E+04	0.9970	0.0368
	347-381	2	y=32.3453-29508.3553x	245.3	3.29E+19	0.9997	0.0206
	381-453	1	y=-1.2580-7805.9082x	64.9	2.22E+04	0.9982	0.0209
MS-800-Char	279-467	1	y=9.1642-14250.4801x	118.5	1.36E+09	0.9968	0.1533
CS	248-320	1	y=0.2049-7661.5994x	63.7	9.40E+04	0.9924	0.0645
	320-422	1	y=-10.3014-1440.2569x	12.0	4.84E-01	0.9928	0.0125
	422-456	1.5	y=48.9080-42120.9377x	350.2	7.33E+26	0.9740	0.1758
CS-300-Char	252-316	1	y=4.0852-10256.9581x	85.3	6.10E+06	0.9943	0.0669

	316-417	1	y=-8.7234-2714.64x	22.6	4.42E+00	0.9981	0.0121
	417-469	2	y=60.2061-49225.0006x	409.3	6.91E+31	0.9735	0.3155
CS-400-Char	306-418	1	y=-7.1561-4026.8249x	33.5	3.14E+01	0.9967	0.0261
	418-482	2	y=38.5144-34800.9785x	289.3	1.85E+22	0.9844	0.2044
CS-500-Char	316-410	1	y=-2.8893-7036.0171x	58.5	3.91E+03	0.9909	0.0653
	410-486	1.5	y=20.3929-22804.6308x	189.6	1.64E+14	0.9922	0.1154
CS-600-Char	333-380	1	y=19.4179-21280.3223x	176.9	5.77E+13	0.9912	0.1081
	380-431	2	y=-3.4584-6023.9427x	50.1	1.90E+03	0.9964	0.0168
	431-491	1.25	y=16.6308-20581.4775x	171.1	3.44E+12	0.9946	0.0661
CS-700-Char	338-380	1	y=19.9027-18078.2613x	150.3	7.96E+13	0.9955	0.0595
	380-431	1.5	y=-3.0649-6118.6910x	50.9	2.85E+03	0.9983	0.0117
	431-479	1	y=10.8639-16369.4511x	136.1	8.55E+09	0.9977	0.0278
CS-800-Char	339-473	1	y=4.757-11817.4847	98.3	1.38E+07	0.9951	0.0964

Figure Captions

Fig. 1. Schematic of (a) three-step carbonization furnace, (b) carbonization tube furnace experiment system.

Fig. 2. Heating temperature profiles of carbonization experiments.

Fig. 3. TG, DTG and DTA profiles of combustion of the raw and carbonized maize straw (MS): (a) TG curves, (b) DTG curves and (c) DTA curves.

Fig. 4. TG, DTG and DTA profiles of combustion of the raw and carbonized cotton stalk (CS): (a) TG curves, (b) DTG curves and (c) DTA curves.

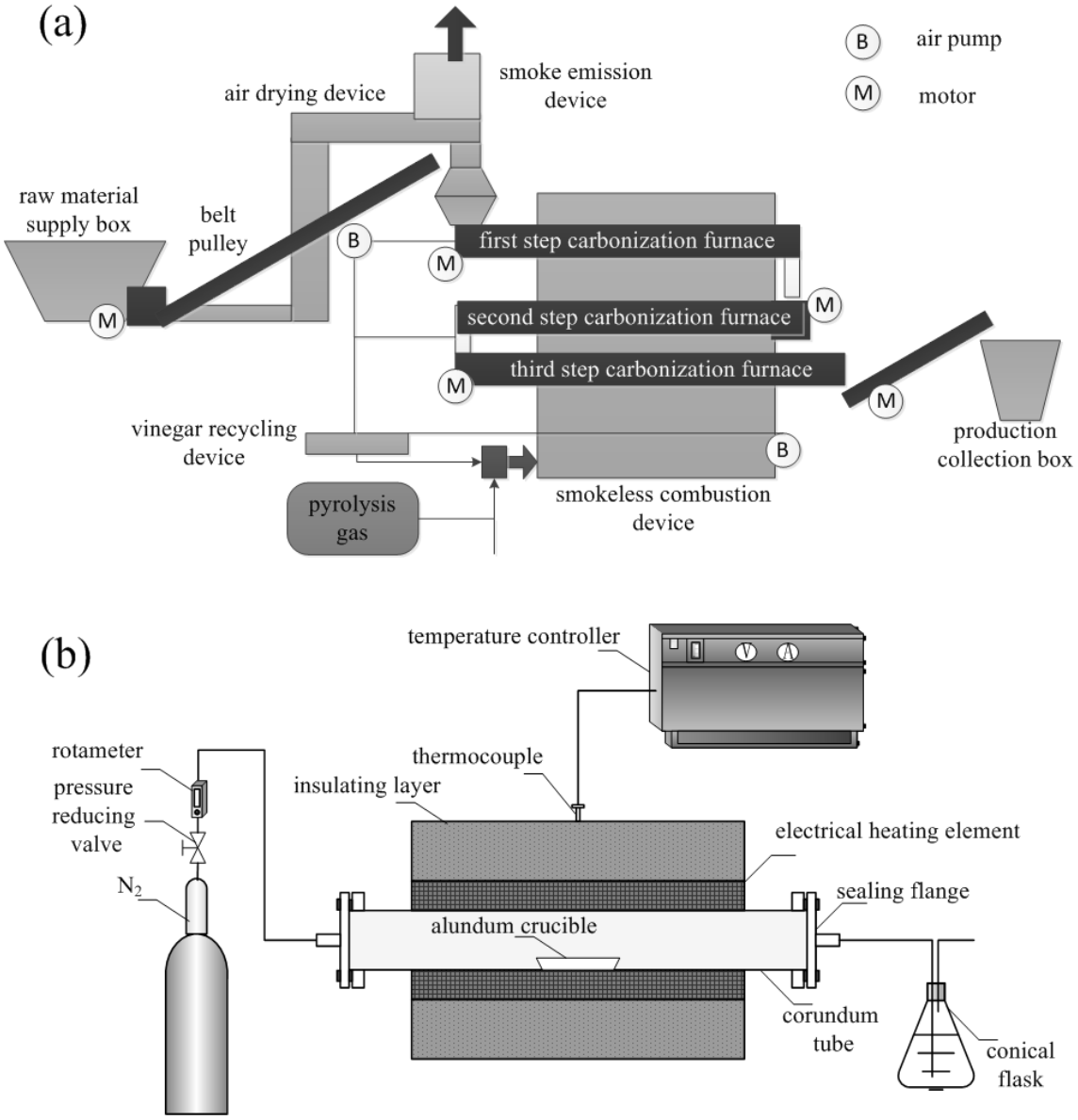

Fig. 1. Schematic of (a) three-step carbonization furnace, (b) carbonization tube furnace experiment system.

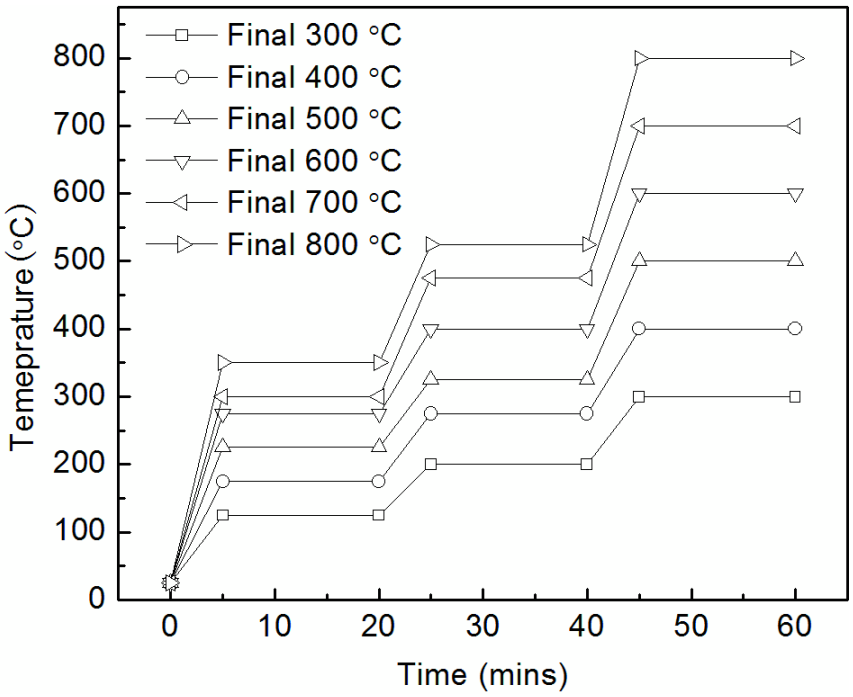

Fig. 2. Heating temperature profiles of carbonization experiments.

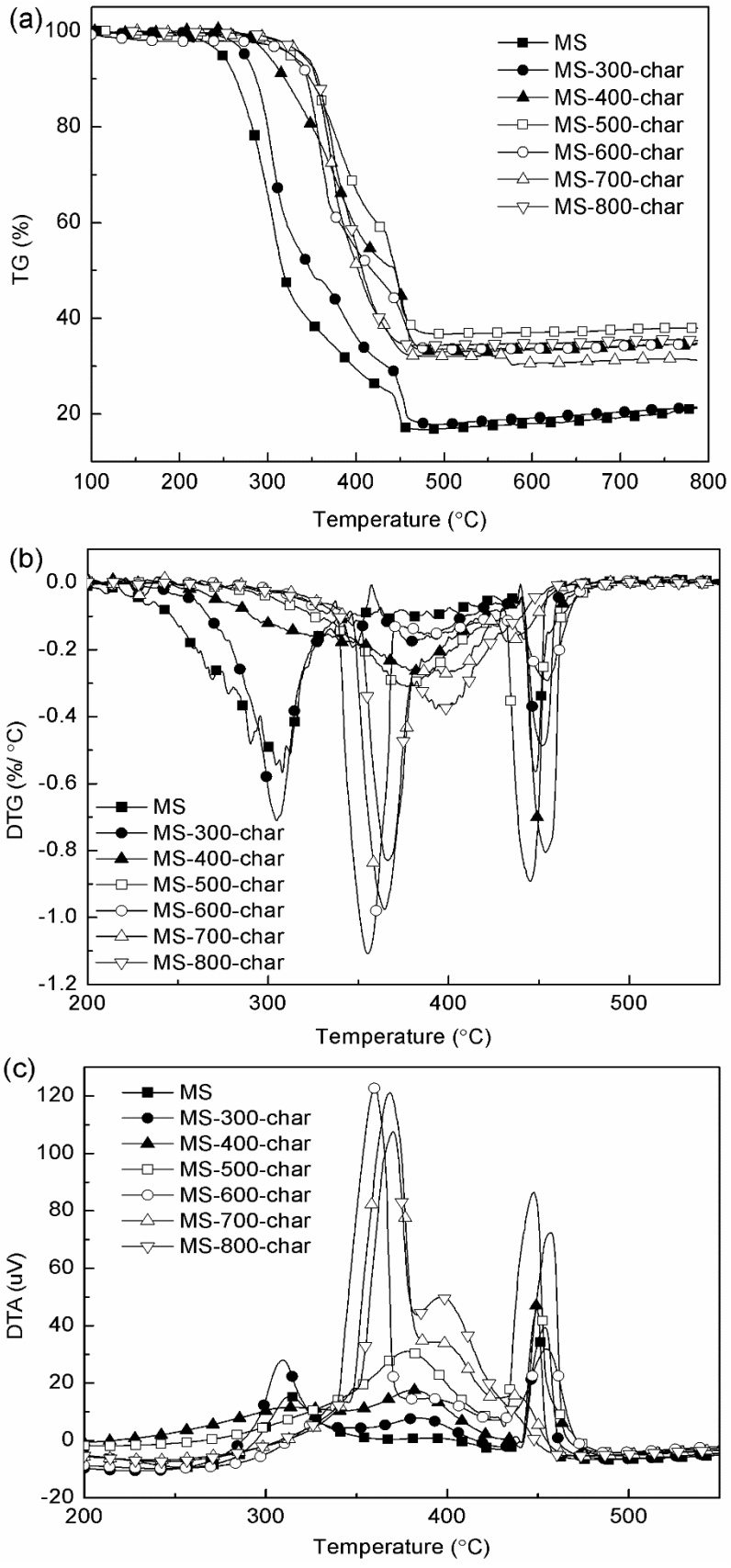

Fig. 3. TG, DTG and DTA profiles of combustion of the raw and carbonized maize straw (MS): (a) TG curves, (b) DTG curves and (c) DTA curves.

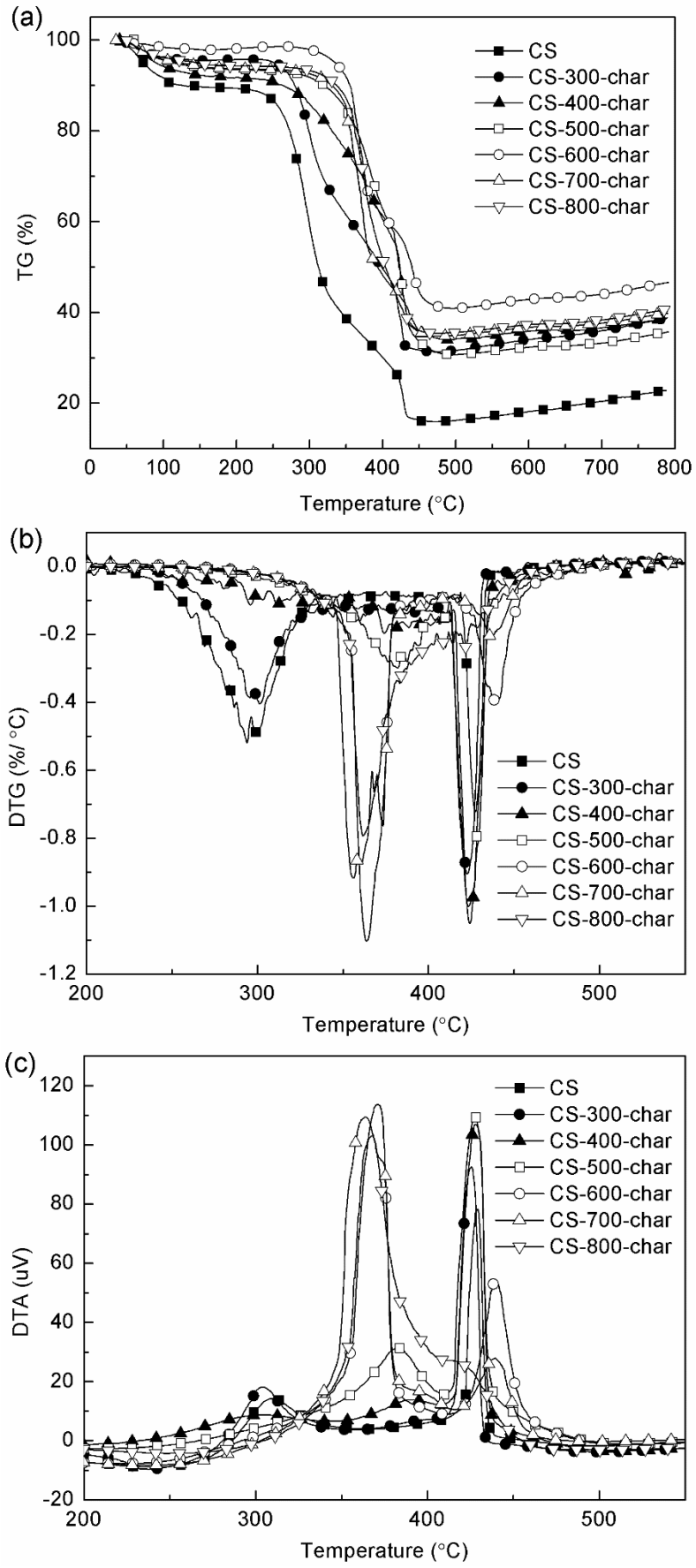
(a)
TG (%)
Temperature (°C)
CS
CS-300-char
CS-400-char
CS-500-char
CS-600-char
CS-700-char
CS-800-char
(b)
DTG (%/ °C)
Temperature (°C)
(c)
DTA (uV)
Temperature (°C)

Fig. 4. TG, DTG and DTA profiles of combustion of the raw and carbonized cotton stalk (CS): (a) TG curves, (b) DTG curves and (c) DTA curves.